Cavitation Number as a Function of Disk Cavitator Radius:

a Numerical Analysis of Natural Supercavitation

Reid Prichard

A Senior Thesis submitted in partial fulfillment
of the requirements for graduation
in the Honors Program
Liberty University
Spring 2019

Acceptance of Senior Honors Thesis

This Senior Honors Thesis is accepted in partial fulfillment of the requirements for graduation from the Honors Program of Liberty University.

_____

Thomas Eldredge, Ph.D.
Thesis Chair

_____

Timo Budarz, Ph.D.
Committee Member

_____

Hector Medina, Ph.D.
Committee Member

_____

James H. Nutter, D.A.
Honors Director

_____

Date

Abstract

Due to the greater viscosity and density of water compared to air, the maximum speed of underwater travel is severely limited compared to other methods of transportation. However, a technology called supercavitation – which uses a disk-shaped cavitator to envelop a vehicle in a bubble of steam – promises to greatly decrease skin friction drag. While a large cavitator enables the occurrence of supercavitation at low velocities, it adds substantial unnecessary drag at higher speeds. Based on CFD results, a relationship between cavitator diameter and cavitation number is developed, and it is substituted into an existing equation relating drag coefficient to cavitation number. The final relationship predicts drag from cavitator radius fairly well, with an absolute error less than 5.4% at a cavitator radius above 14.14mm and as low as 1.3% at the maximum tested radius of 22.5mm.

Keywords: *supercavitation, cavitation number, disk cavitator, CFD, multiphase flow*

Table of Contents

A Numerical Analysis of Natural Supercavitation

Background

In outer space, the Apollo 10 capsule hit a peak speed of 24,790 mph. Within Earth's atmosphere, the X-15A-2 jet set the airspeed record of 4,520 mph. On land, the ThrustSSC jet car reached 763 mph. Even on the water, the Spirit of Australia set a record of 318 mph. Underwater, though, rumors suggest that the top speed ever reached by a manned craft (while its true value is classified) is just over 50 mph. This disparity is largely due to the properties of water. At 20°C, its dynamic viscosity is nearly two orders of magnitude greater than air's, leading to correspondingly greater skin friction drag. Consequently, any method to reduce skin drag would have significant implications on the speed and efficiency of underwater travel.

In the 1960s, the Soviet Union began research into a technology called supercavitation, which they began applying to a high-speed torpedo. While cavitation is typically avoided, supercavitation leverages the phenomenon to reduce drag. Supercavitation consists of the use of a sharp-edged shape at the front of the vehicle (such as a flat disk; this is known as the cavitator) to reduce the static pressure of the water as it flows past. If the velocity is high enough, the local water pressure will drop below the vapor pressure and cause the water to boil. Because of the motion of the vehicle, the steam produced by the cavitator will extend backwards and (again, only if the vehicle is traveling fast enough) envelop the vehicle with a bubble of steam referred to as a *supercavity*. Since the viscosity of steam is around two orders of magnitude less than the viscosity of liquid water, this allows a high rate of shear with much less frictional drag force. However, a large-diameter cavitator is necessary to generate a supercavity of

steam, and pushing a large bluff body through water at a high rate creates substantial pressure drag.

To date, supercavitation has only been implemented on small objects such as torpedoes and projectiles, partially because increasing the size of the supercavitating object greatly increases the propulsive power required. To achieve the ultimate application—a supercavitating submarine—supercavitation must be made more efficient. This can be accomplished by ventilating the supercavity with non-condensable gas, designing a more effective cavitator (or utilizing multiple cavitators over the length of the vehicle), or even heating the cavitator to increase the saturation pressure.

Cavitation Number

Supercavitation is often analyzed with a dimensionless constant called the cavitation number σ, which is defined as:

$$\sigma = \frac{P_0 - P_{cavity}}{\frac{1}{2}\rho_0 u_0^2} \tag{1}$$

where P_0, ρ_0, and u_0 are the static pressure, density, and velocity of the free stream, and P_{cavity} is the static pressure inside the cavity. The cavitation number in a supercavitating flow is typically less than 0.1, the values measured in this study are mostly in the range of $0.02 < \rho < 0.05$. While it is hard to compare different geometries with geometric parameters, cavitation number can be used to compare different supercavitating geometries and setups, and empirical relationships are typically found with cavitation number as the independent variable. For example, the behavior of the closure area of a

supercavity is a function of the product of the Froude number and the cavitation number. (Skidmore, Brungart, Lindau, & Moeny, 2016). Furthermore, an empirical relationship has been found giving drag coefficient as a function of cavitation number (May, 1975).

Natural Supercavitation

Natural supercavitation uses an unaided cavitator to generate the supercavity. While simpler than other alternatives, natural supercavitation causes a large amount of pressure drag due to the large cavitator required. This can be worthwhile in certain cases where simplicity is key, such as supercavitating ammunition, but larger applications require less drag.

Ventilated Supercavitation

Ventilated supercavitation uses a cavitator like natural supercavitation, but it makes one addition. An inert gas such as compressed air or carbon dioxide is injected into the supercavity through nozzles on the cavitator. The addition of a gas decreases the partial pressure of the water vapor, which allows the cavity to be sustained at a lower cavitation number (i.e. a higher cavity pressure). The important consequence is that ventilation allows a stable supercavity to form with the use of a smaller cavitator, which greatly decreases pressure drag. This technique has been exploited in Russia's VA-111 Shkval (Squall) torpedo, which is able to travel underwater at over 230 mph.

Geometry

The test subject used in this study was based loosely on the VA-111 Shvkal, The geometry of its nose section is shown in Figure 1. This study varies the radius of the cavitator (depicted as *r* in the inset) as its independent variable.

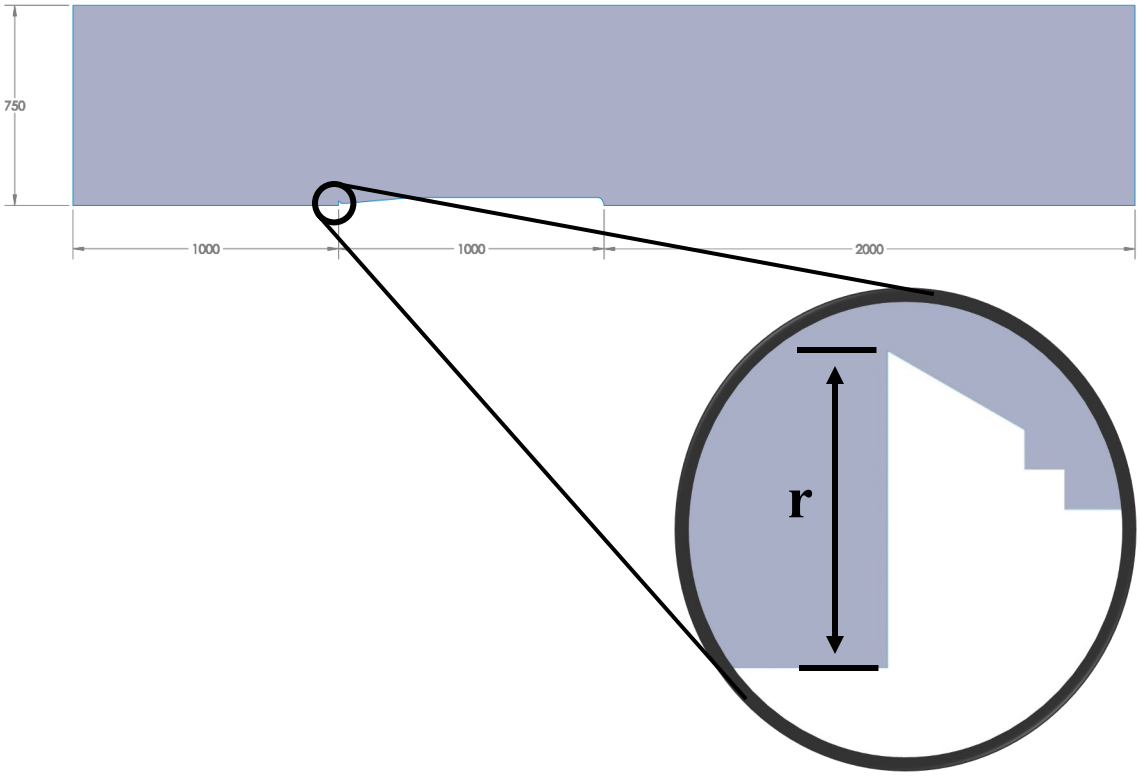

Figure 1. Supercavitating underwater vehicle geometry. Inset shows cavitator head with parameter of study, r. Dimensions in mm.

Meshing

Meshing was performed using ANSYS Workbench 18.2's build-in meshing tool. Most of the default mesh settings were kept, but a few options were changed to refine the mesh. *Relevance* (a parameter used by ANSYS to control mesh fineness) was set to its maximum value (100) and *relevance center* to "fine" (*relevance center* works in conjunction with *relevance* to control fineness), although the refinement imposed by sizing controls likely made this irrelevant.

A parameterized edge sizing was added on all edges of the torpedo, which specified a fixed element edge size along its surface. The value of this parameter was optimized in the mesh independence study. The global maximum face size was defined according to the following equation:

$$s_f = c_s s_e \tag{2}$$

where s_f is the value of the face sizing parameter in mm, c_s is the sizing ratio coefficient, and s_e is the value of the edge sizing parameter in mm. Furthermore, *target skewness* was decreased from the default value of 0.9 to 0.5, and *smoothing* was increased from "medium" to "high." These settings added an insignificant amount to the meshing time (compared to the overall simulation time), and a subjective visual analysis indicated they increased mesh quality.

Lastly, an *inflation* was added to the entire surface of the torpedo. As shown in Figure 2 and Figure 3, an inflation layer transforms a layer of cells along a surface into progressively-smaller rectangular cells, which allows the simulation to better resolve the boundary layer.

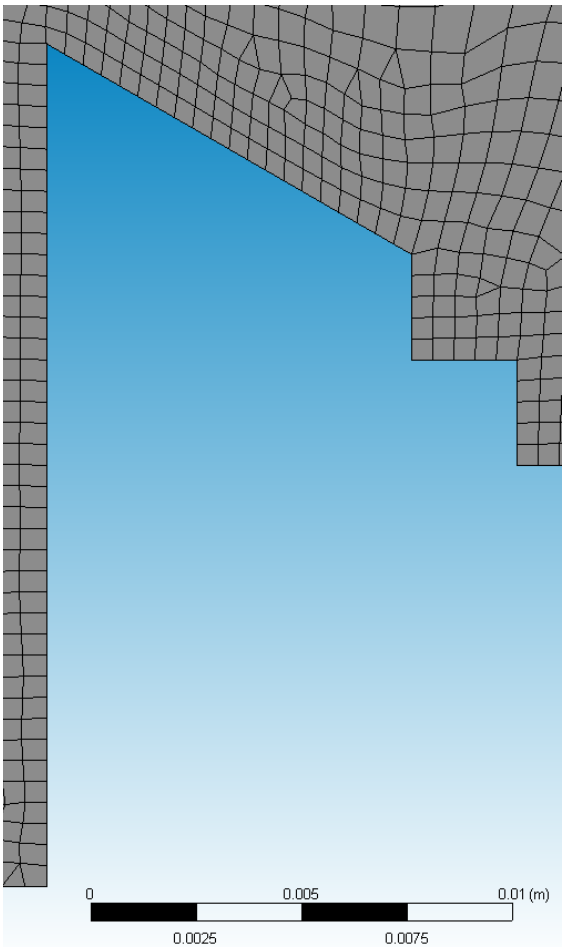

Figure 3. Sample mesh of cavitator head with inflation layer disabled.

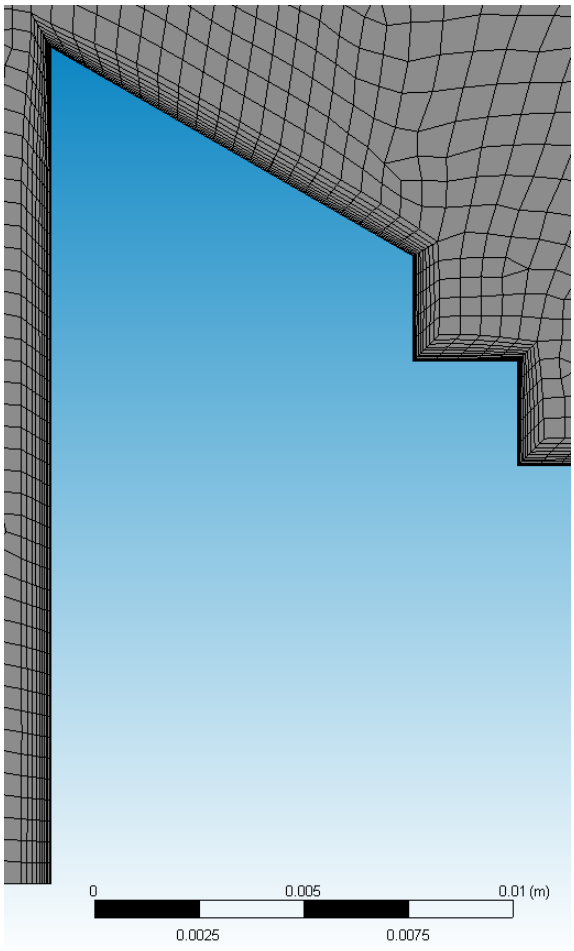

Figure 2. Sample mesh of cavitator head with inflation layer enabled.

Mesh Independence Study

After setting up the framework of the simulation, it was necessary to determine the mesh resolution required to accurately model the effects at play. Initially, this was done by varying only the edge sizing on the torpedo's body, but it was found that the mesh element size in the free stream significantly affected parameters of interest. Adding a second degree of freedom complicated finding mesh independence. After some initial experimentation to determine the range of values to analyze for the edge sizing and the mesh size ratio, a series of 23 simulations was created and run. These 23 simulations

consisted of every permutation of the two parameters listed in Table 1. An additional two simulations used edge sizing values of 0.354mm and 0.25mm, both at a size ratio of 15. The permutations are listed in Appendix A.

Table 1

Mesh independence study parameters.

Parameter 1 – edge sizing	Parameter 2 – mesh size ratio
0.5mm	5
0.707mm	7.07
1mm	10
	14.14
	20
	28.28
	40

Courant Number

In time-dependent computational flows, the Courant number is an important dimensionless parameter. The Courant number is defined as:

$$C = \frac{u\,\Delta t}{\Delta x} \tag{3}$$

where u is the magnitude of the velocity, Δt is the time step, and Δx is the grid spacing (approximately the edge length of a cell in the mesh). It is important that $C \leq 1$; if the

Courant number is greater than one, the flow will pass through more than one cell in a single time step, which can reduce accuracy or cause a simulation to diverge.

Based on this requirement, the time step was set to aim for C = ½. The following equation was used to attempt to achieve this value of Courant number:

$$\Delta t = \frac{s_e}{2 \times v_{inlet}} \tag{4}$$

where s_e is the value of the edge sizing parameter ($s_e \approx \Delta x$), and v_{inlet} is the prescribed inlet velocity. An inspection of a contour plot of Courant number revealed that this condition successfully resulted in C ≈ ½ along the surface of the torpedo, although a few cells at the edge of the cavitator had a Courant number of 3 to 4 due to the higher local velocity. While undesirable, this did not negatively affect the simulation's stability.

Y-Plus Value

Another important value to consider in CFD is the dimensionless wall distance, y^+. The y^+ value is defined as:

$$y^+ = \frac{\sqrt{\frac{\tau_w}{\rho}} \times y}{\nu} \tag{5}$$

where τ_w is the wall shear stress, ρ is the fluid density at the wall, y is the absolute distance to the nearest wall, and ν is the local kinematic viscosity of the fluid (Schlichting & Gersten, 2001). The y^+ value indicates how well-resolved a boundary layer is. As a general guideline, it is suggested to keep y^+ in the range of $30 < y^+ < 300$. If y^+ is too

small, over-resolution of the boundary layer can interfere with the turbulence model's wall function. On the other hand, if y^+ is too large, important detail will be lost. As with the Courant number, the high velocity over the leading edge of the cavitator initially resulted in large y^+ values; the y^+ was reduced by adding the previously-mentioned inflation layer to the mesh. However, it was observed that reducing the y^+ value tends to increase the Courant number, so a balance had to be struck between the two.

Error Analysis

Once the simulations were completed, Microsoft Excel was used to analyze the data. The reciprocal of the number of elements in each design point was compared with the parameters of interest (drag force, cavitation number, and steam volume fraction) using Excel's built-in linear regression. The values of the output parameters as mesh element count goes to infinity are of interest, and these values correspond to the reciprocal of element count going to zero. This value is represented by the intercept of the regression and will be referred to as the mesh-independent parameter value. These plots are shown in Figure 4 through Figure 6.

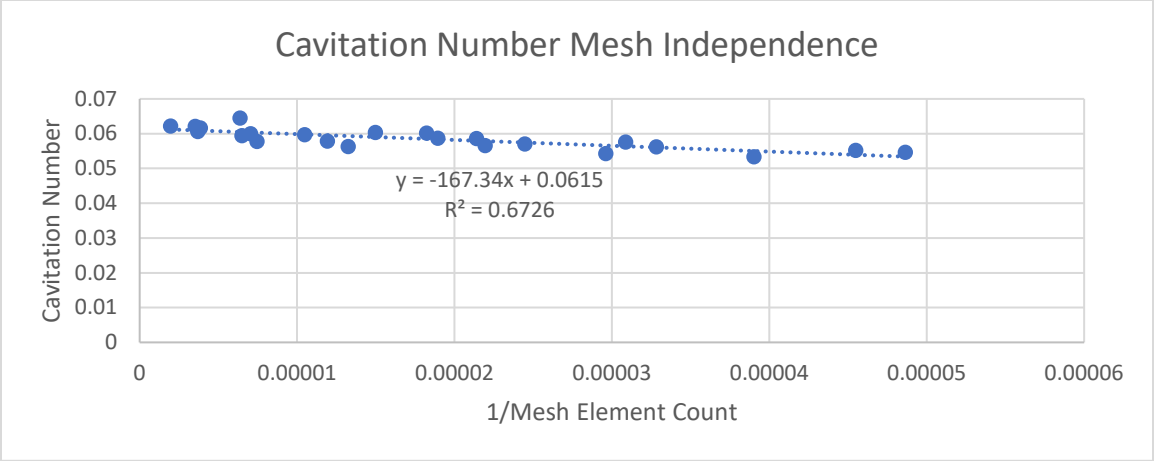

Figure 4. Cavitation number mesh independence plot.

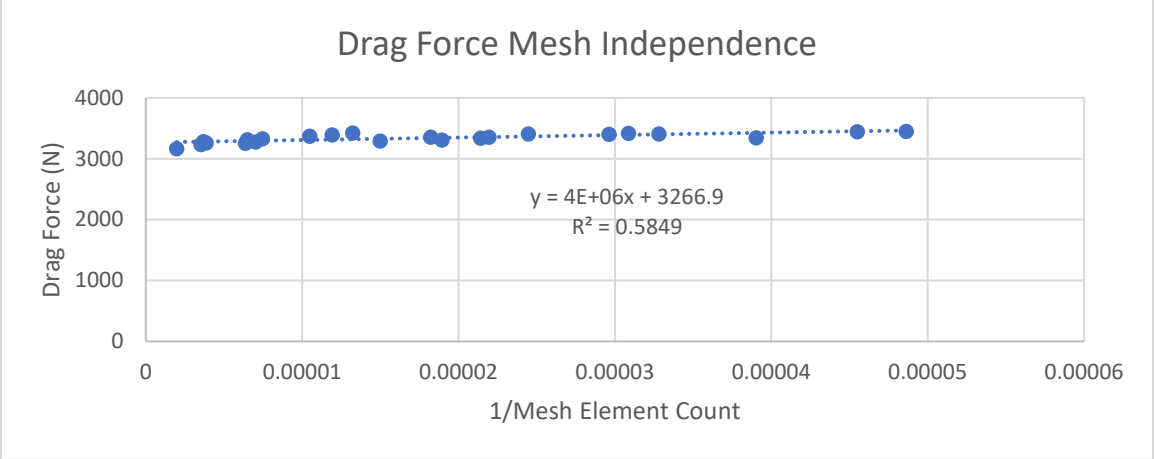

Figure 5. Drag force mesh independence plot.

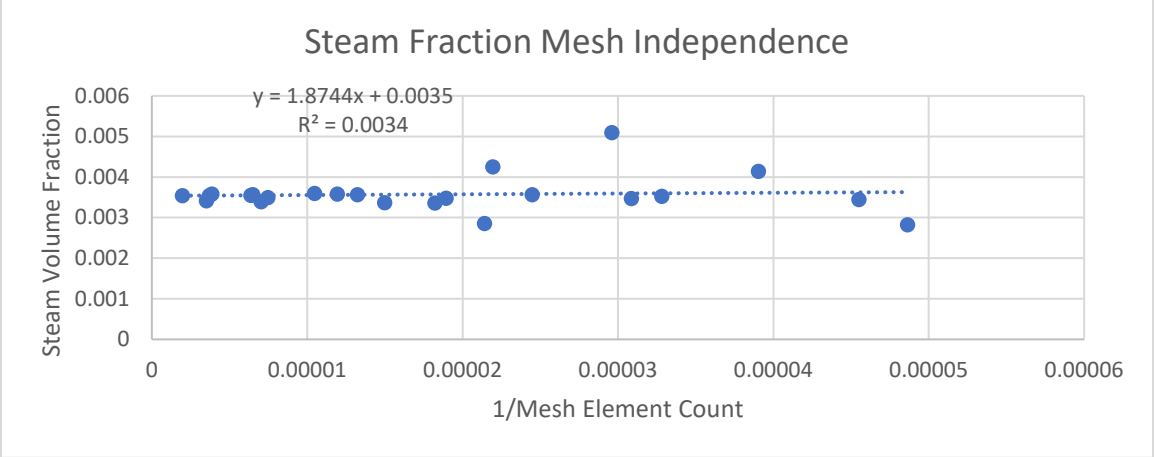

Figure 6. Steam fraction mesh independence plot.

The absolute error was then calculated for each parameter at each design point.

$$\text{Error} = \left| \frac{\text{parameter value}}{\text{mesh-independent parameter value}} - 1 \right| \tag{6}$$

Even the finest mesh tested, with over 500,000 elements, showed errors of a few percent in the output parameters, indicating failure to reach a truly mesh-independent simulation. However, computational limitations prevented the use of larger meshes, so the data were analyzed to find the best compromise between performance and accuracy.

The AVERAGEIF function was used to find the average mesh size and the average absolute error of each parameter for each body sizing and size ratio value. These data are shown in Table 2. Note in Appendix A that the two smallest torpedo body mesh sizes each only corresponded to a size ratio of 15, and those were the only design points that used the size ratio of 15, so those rows in Table 2 should not be expected to follow trends seen in other values.

Additionally, the error in each parameter versus the mesh element count was plotted to visually compare the mesh sizes. Because two mesh parameters were being varied, these data were not as smooth as one might expect, but they were helpful in looking for outliers. A regression line was added to each plot, which allowed quick judgment of whether a mesh was more efficient or less efficient based on whether it fell above or below the line. In can be seen in Figure 7 through Figure 9 that the chosen parameters achieved a good compromise between mesh size and error. While several other points appear promising, some meshes introduced significant performance issues.

Table 2

Averaged absolute error as function of varying input parameters.

		Elements	Cavitation number	Drag force	Steam volume fraction
Body Sizing (mm)	0.25	283919	1.0%	1.0%	3.5%
	0.354	156651	4.7%	0.3%	0.2%
	0.5	170252	3.4%	1.9%	4.2%
	0.707	92198	5.5%	2.9%	8.1%
	1	50981	8.7%	3.9%	9.0%
Size Ratio	5	300021	2.5%	1.7%	0.8%
	7.07	162847	4.1%	1.9%	1.6%
	10	94778	4.7%	2.6%	7.1%
	14.14	60897	3.9%	3.5%	2.9%
	15	220285	2.8%	0.6%	1.9%
	20	44416	7.6%	2.6%	7.5%
	28.28	36182	8.9%	3.6%	16.1%
	40	32198	9.4%	4.3%	13.5%

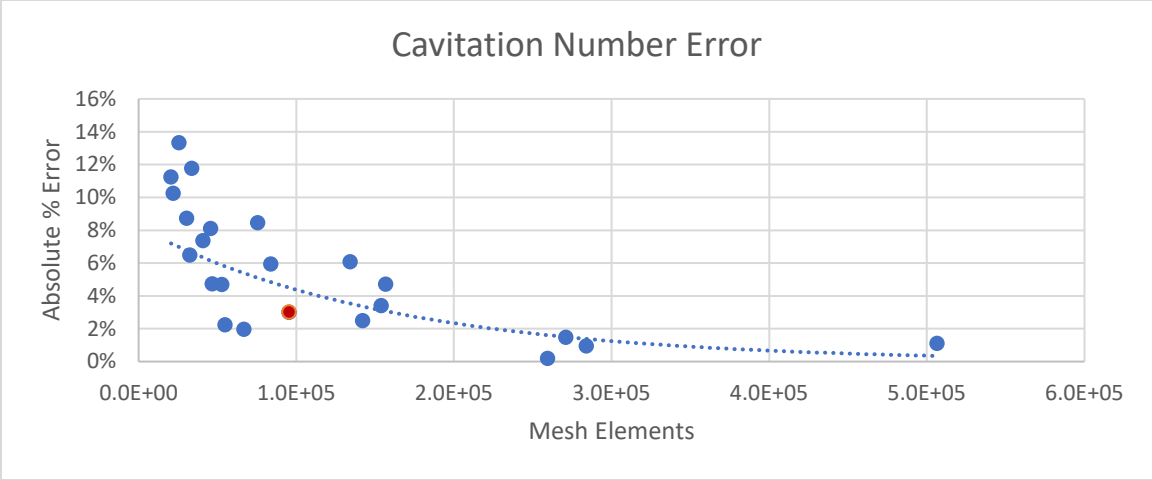

Figure 7. Error in cavitation number versus mesh element count. Red datapoint indicates parameters chosen for study.

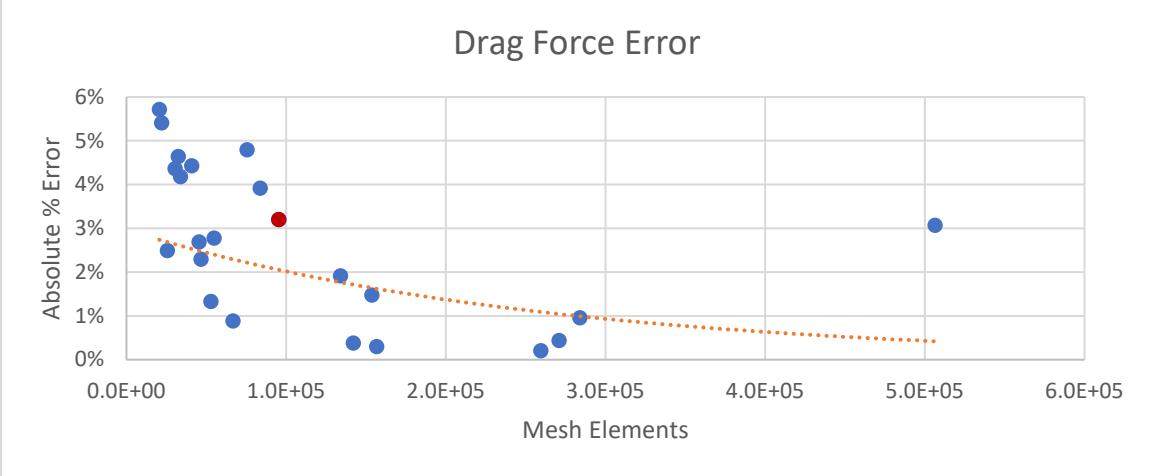

Figure 8. Error in drag force versus mesh element count. Red datapoint indicates parameters chosen for study.

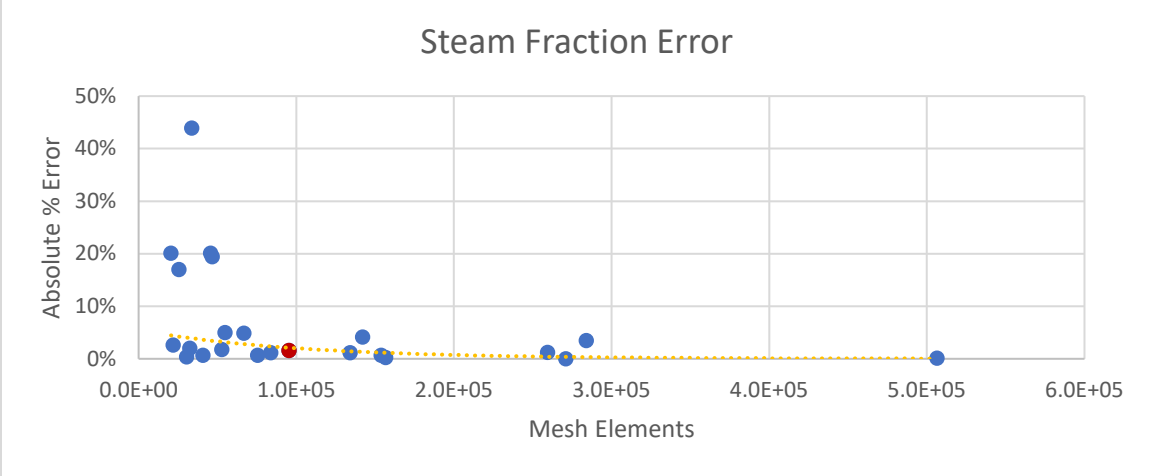

Figure 9. Error in steam volume fraction versus mesh element count. Red datapoint indicates parameters chosen for *study.*

Based on the values in Table 2, it was decided that the best compromise between mesh size and accuracy was presented by a body sizing of 0.5mm and a size ratio of 14.14, which was rounded to 15 for final simulations.

Time step Independence Study

Once the mesh independence study was complete, it was necessary to conduct a time step independence study. Up until this point, the time step had been set as defined in Equation 4 to achieve a Courant number of 0.5 on the torpedo's surface (which should be the location of the smallest cells). An additional study with identical parameters was performed, except the time step was doubled. As shown in Table 3, the difference between the two time steps was negligible, indicating that either condition was sufficient for time step independence.

Table 3

Time step independence study results.

Time step	**Steam fraction**	**Drag force**	**Cavitation number**
$\frac{\Delta x}{2 \times v_{inlet}}$	$9.56 * 10^{-4}$	$3.82 * 10^{3}$	.0426
$\frac{\Delta x}{v_{inlet}}$	$9.59 * 10^{-4}$	$3.80 * 10^{3}$	.0429
% difference	0.29%	-0.41%	0.56%

Study Setup

Configuration

The simulations for this study were conducted in ANSYS Fluent 18.2. Because the machine used to perform the calculations had a CPU with 6 physical cores, Fluent

was run in parallel mode with 5 threads. This left one core completely free for background activities, while fully utilizing the remaining physical cores. Though the CPU had two logical processors per physical core, utilizing more than one processor per core slowed computations. It is conjectured this was the case because both logical processors in each physical core share a single memory cache. Additionally, double precision was enabled, because doing so exhibited no penalty to performance and could theoretically produce improvements to precision.

To make the most of limited computational resources, the study was modelled axisymetrically using a 2-dimensional mesh, resulting in far fewer elements than a corresponding 3D mesh. One limitation of the axisymmetric model is that it neglects the effects of buoyancy, but this was determined to be unimportant. In studies of supercavitation, the Froude number is often used to determine the importance of buoyancy. The Froude number is defined as:

$$\mathrm{Fr} = \frac{u_0}{\sqrt{g_0 l_0}} \tag{7}$$

where u_0 is the free stream velocity, g_0 is the gravitational acceleration, and l_0 is the characteristic length. Data suggest that buoyant effects become insignificant as the Froude number increases above approximately 20 (Ahn, et al., 2017). In this case, the Froude number was calculated to be 23.9, so the effects of buoyancy were determined to be insubstantial enough to ignore.

Computational Models

Cavitation was modeled with the VoF (Volume of Fluid) multiphase model. The Standard K-Epsilon turbulence model was used, and the scalable wall function was chosen to allow use of high-density meshes without error.

Boundary Conditions

The left edge of the domain was designated as a velocity inlet with a velocity of 75 m/s, and the right edge was set as a pressure outlet at a relative pressure of 0 atm. The implication of zero relative pressure is that the supercavitating vehicle is traveling arbitrarily close to the water's surface. Realistically, a supercavitating vehicle would travel at least several feet under the water, so the results of this study indicate a bounding value of the largest supercavity size. The bottom edge of the domain was set as an axis of symmetry, and the top edge was left a standard stationary wall.

Convergence Criteria

Simulation convergence was set to be automatically determined in Fluent. The continuity residual convergence criterion was decreased from its default value to 10^{-5}. Additionally, convergence criteria were added to determine overall simulation convergence after a sufficient number of time steps. These criteria were added on all three output parameters – drag force, steam volume fraction, and cavitation number. Cavitation number and drag force were both given a stop criterion of $5 * 10^{-4}$, and steam volume fraction was given a stop criterion of 10^{-5}. These criteria put limits on the maximum proportional variation of each parameter from time step to time step before convergence is achieved. Additionally, each was set to use ten time steps, which ensures that each parameter is stable for at least that many steps. Trial and error revealed that

evaluating parameters at multiple time steps was crucial, as using only a single time step could lead to a false indication of convergence due to a random momentary stabilization in output parameters. Lastly, the cavitation number criterion was set to ignore the first one thousand time steps to prevent convergence from occurring prematurely. This meant that after one thousand time steps had passed, the simulation would complete once each of the three parameters was found to vary less than a proportion of 10^{-5} over 10 time steps.

Fluent User-Defined Function

While running early simulations, it was observed that drag force and the cavitation number both converged to their final value quite quickly, but the steam volume fraction continued to change for much longer. Inspection of a contour plot of the steam volume fraction as the study ran revealed that these changes were largely due to minor variations in steam distribution behind the rear of the torpedo; drag force and cavitation number were steady because the supercavity had already formed. Fluent's variable time-stepping was evaluated, but significant improvement in simulation time was not observed. Instead, a user-defined function (UDF) defining Fluent's DEFINE_DELTAT function was written, which allowed fine-grained control over the time step. The initial UDF was rudimentary: as flow time increased, it would incrementally increase the time step.

```
#include "udf.h"

DEFINE_DELTAT(variable_delta_t,d)
{
  real time_step;
  real inlet_velocity = RP_Get_Input_Parameter("real-1");
  real input_timestep = RP_Get_Input_Parameter("real-2");
  real flow_time = CURRENT_TIME;
  if (flow_time < 1/inlet_velocity)
      time_step = input_timestep;
  else if (flow_time < 2/inlet_velocity)
      time_step = 2*input_timestep;
  else if (flow_time < 3/inlet_velocity)
      time_step = 3*input_timestep;
  else
      time_step = 4*input_timestep;
  return time_step;
}
```

Figure 10. UDF version 1.

This solution was far from optimal, though. In general, it tended to decrease computation time, but in certain cases which required a long time to settle (such as cases with a large cavitator disk and a high inlet velocity), it would increase simulation time tremendously or even cause the simulation to diverge. To circumvent this, a new UDF was written that intelligently adjusted the time step. It was programmed to dynamically adjust the time step in pursuit of twenty iterations per time step. It would increase the time step if the iterations per time step were significantly less than 20 and decrease the time step if the iterations per time step were significantly greater than 20. However, since this is a purely proportional control, a positive feedback loop would cause undesirable

oscillations. Ultimately, these would crash Fluent as the time step approached zero on the low end.

In attempt to find a happy medium, aspects of the two UDFs were combined, creating one that would increment the time step like the first UDF, but only if the number of iterations per time step were significantly less than 20. (It would not decrease the time step.) While this UDF did not crash Fluent and appeared to reduce simulation time, it produced results significantly different than simulations run with a fixed time step, so the use of a UDF was ultimately abandoned. Future studies might explore a similar UDF that reverted to the original time step as the study appeared to near convergence.

```
#include "udf.h"
#include "unsteady.h"
static int iters = -1;
static int prev_iters = -1;
DEFINE_DELTAT(variable_delta_t, d)
{
    real time_step;
    real inlet_velocity = RP_Get_Input_Parameter("real-1");
    real input_timestep = RP_Get_Input_Parameter("real-2");
    real flow_time = CURRENT_TIME;
    const int target_iters = 20;
    if (N_ITER != prev_iters)
    {
        prev_iters = iters;
        iters = (int)N_ITER;
        iters = (nres == 0) ? (0) : ((int)count2[nres - 1]);
    }
    int delta_iters = iters - prev_iters;
    time_step = input_timestep;
    if ((flow_time < 2/inlet_velocity) && (delta_iters < 0.5 * target_iters))
    {
        time_step = input_timestep * 2;
    }
    else if ((flow_time < 3/inlet_velocity) && (delta_iters < 0.5 *
target_iters))
    {
        time_step = input_timestep * 3;
    }
    return time_step;
}
```

Figure 11. Final, revised version of DEFINE_DELTAT UDF.

Simulation Data

In the final simulations, a body sizing of 1mm and mesh size ratio of 15 were used, as previously mentioned. The inlet velocity remained 75 m/s, and the cavitator radius was varied from 5mm to 22.5mm as shown in Table 4.

Table 4

Design points

Design point	Cavitator radius (mm)
DP 0	5
DP 1	7.07
DP 2	10
DP 3	14.14
DP 4	16.82
DP 5	20
DP 6	22.5

The resulting data yielded the chart shown in Figure 12.

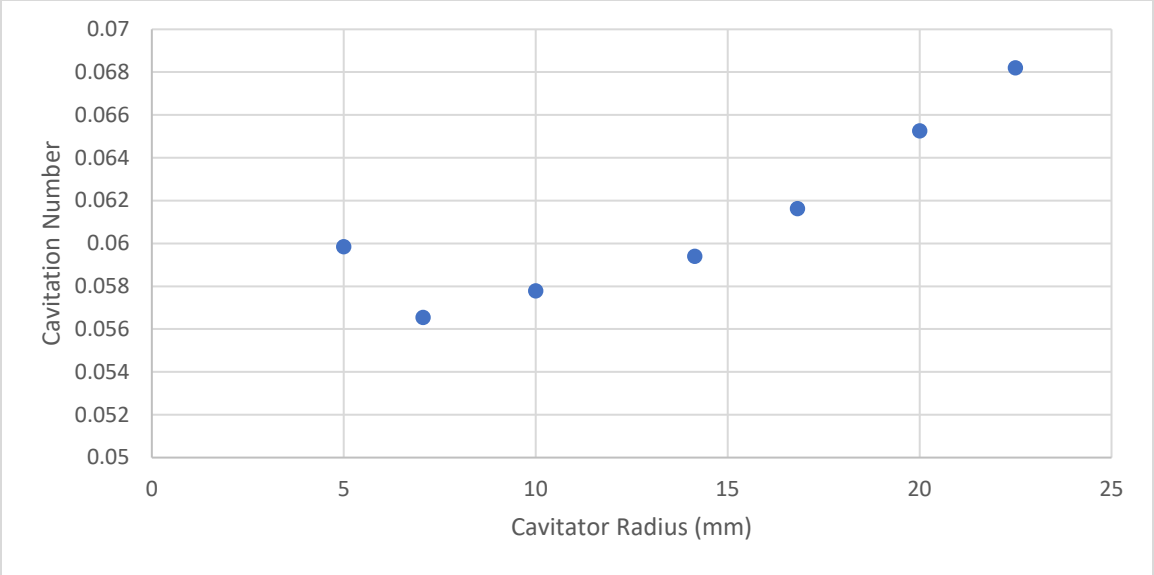

Figure 12. Raw simulation data comparing cavitation number and cavitator radius.

Results and Analysis

Knowledge of supercavitation results in the conclusion that cavitation number should not increase with decreasing cavitator radius as suggested by the leftmost datapoint. Because the simulation would diverge with radii any lower than 5mm, and the 5mm datapoint clearly violated the trend, it was discarded, and the data reanalyzed, as shown in Figure 13.

In attempt to model the simulation data, a polynomial trendline was fit to the data in Excel. As shown in Figure 13, the second-degree trendline appears to represent the trend well and exhibits an appealing R^2 value of 0.9975. However, the trendline violates the behavior expected in which cavitation number decreases as it approaches the ordinate axis.

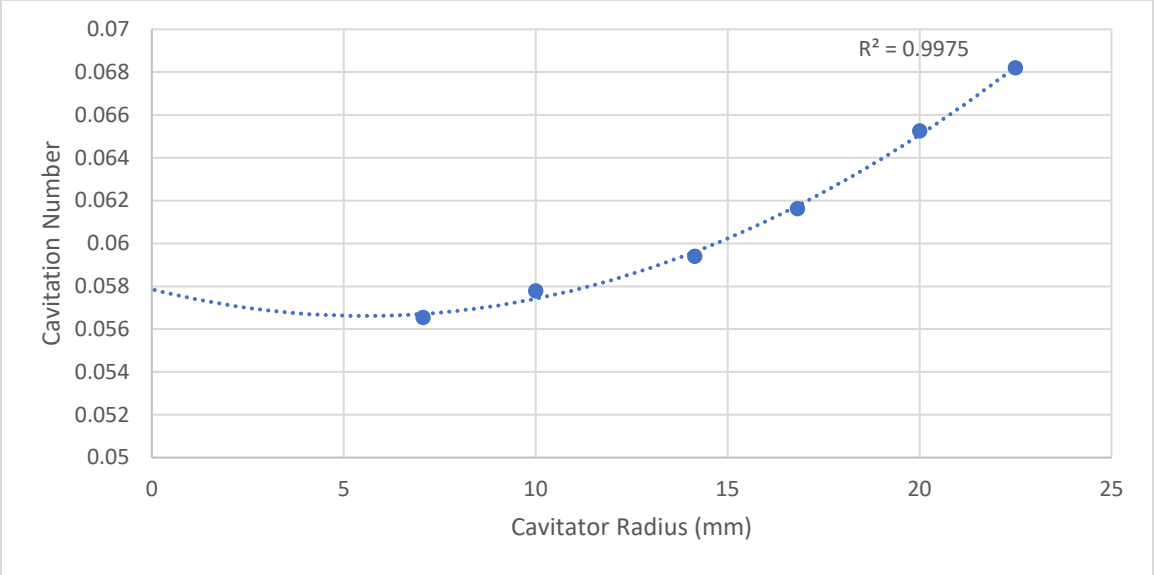

Figure 13. Simulation data with 5mm datapoint discarded. $R^2 = 0.9975$

In attempt to make better sense of the data, MATLAB's Curve Fitting Toolbox was utilized. Using a 2-term power regression resulted in the trendline shown in Figure 14, which is described by:

$$\sigma = 1.6246 * 10^{-5} r^{2.1406} + 0.055219 \quad (8)$$

This final regression follows the expected trend down to r = 0, so it is determined to be an acceptable model.

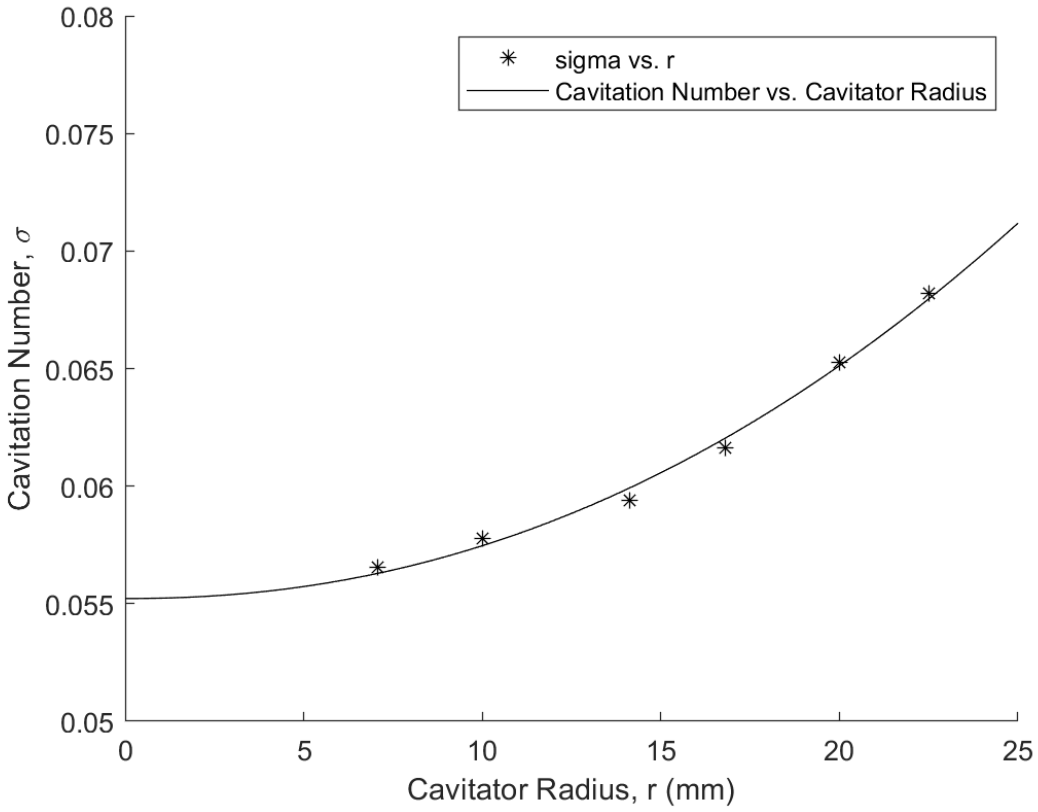

Figure 14. Two-term power regression of cavitation number vs cavitator radius as described in Equation 8.

Existing literature gives the relationship (May, 1975):

$$C_D = 0.815(1 + \sigma) \tag{9}$$

where C_D is the drag coefficient. In fluid mechanics, drag force is commonly defined according to the following equation:

$$F_D = \frac{1}{2} C_D A \rho u_0^2 \tag{10}$$

where A is the frontal area of the object, ρ is the fluid density, and u_0 is the free stream

fluid velocity. Equation 10 can be combined with Equation 9 to yield:

$$F_D = 0.4075(1+\sigma)\,\pi \mathrm{r}^2 \rho\, u_0^2 * 10^{-6} \tag{11}$$

where F_D is the drag force in N, r is the radius in mm, ρ is the density in $\frac{\mathrm{kg}}{\mathrm{m}^3}$. Substituting Equation 8 into Equation 11 yields:

$$F_D = 2.07981 * 10^{-11} \rho u_0^2 (r^{4.1406} + 64952.5\, r^2) \tag{12}$$

At lower values, the final relationship does not agree with data taken. At the smallest cavitator diameter tested, Equation 12 underestimates drag force by 84.9% compared to the simulated value. As cavitator diameter increases, though, the error sharply decreases. By r = 14.14mm, the error is just -5.4%, and at r = 22.5mm it is just -1.3%. It is conjectured that partial supercavitation does not follow the trend found by May but that it is an accurate representation once the supercavity envelops the vehicle.

Table 5

Drag force data comparing theoretical value to measured value.

ρ	C_D	r (mm)	A_{pl} (mm^2)	V (m/s)	Predicted F_D (N)	Simulation F_D (N)	% difference
0.0599	0.864	5	78.5	75	190.1	1256.9	-84.9%
0.0565	0.861	7.07	157.0	75	380.2	1234.6	-69.2%
0.0578	0.862	10	314.2	75	761.5	1229.5	-38.1%
0.0594	0.863	14.14	628.1	75	1526.1	1612.9	-5.4%
0.0616	0.865	16.82	888.8	75	2163.7	2207.8	-2.0%
0.0653	0.868	20	1256.6	75	3068.0	3114.0	-1.5%
0.0682	0.871	22.5	1590.4	75	3893.3	3946.3	-1.3%

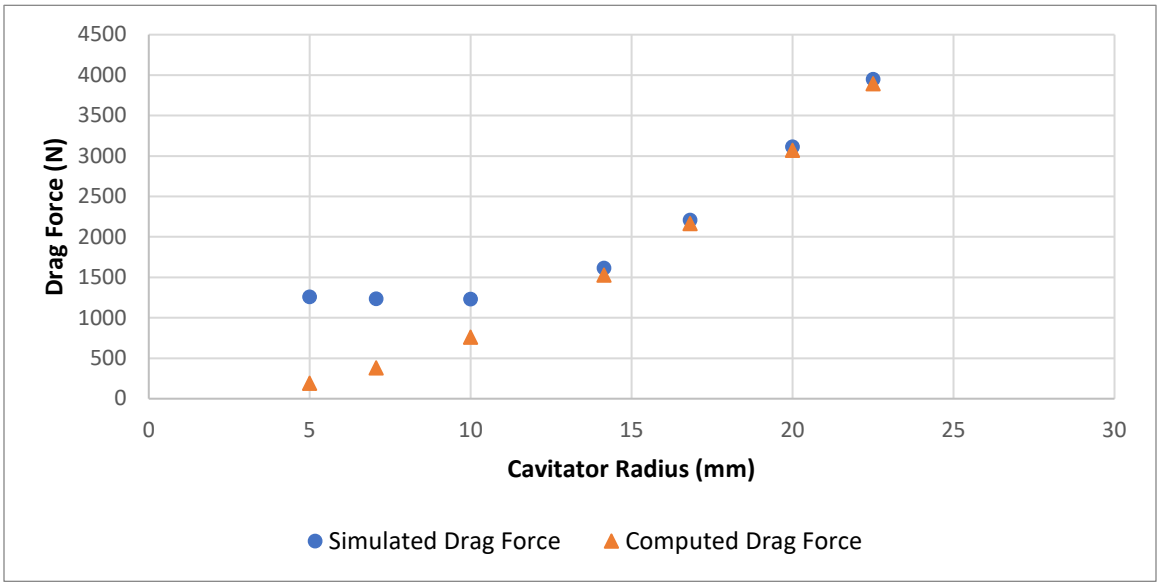

Figure 15. Comparison of drag force calculated in Fluent simulations versus drag force predicted using Equation 12.

Conclusions

The final relationship between cavitator radius and drag force shows inaccuracy at lower radii, but its relatively low error in the full supercavitation regime is surprising given the suboptimal meshes used for this study. Since the primary obstacle was lack of computational resources, a more accurate relationship could be found if these simulations were repeated with higher-quality meshes.

As it stands, the discovered relationship could serve as a useful tool to predict cavitation number and drag coefficient of a torpedo-style vehicle with a disk cavitator operating in natural supercavitation.

Further avenues of research could include examining a broader range of cavitator radii, performing simulations at varying inlet velocities, and performing a control simulation without a cavitator. Additionally, further analysis could explore the origins of the discovered empirical relationship, and perhaps even find an analytical relationship.

References

Ahn, B.-K., Jeong, S.-W., Kim, J.-H., Shao, S., Hong, J., & Arndt, R. E. (2017). An experimental investigation of artificial supercavitation generated by air injection behind disk-shaped cavitators. *International Journal of Naval Architecture and Ocean Engineering, 9*(2), 227-237.

Ahn, B.-K., Jung, S.-W., Kim, J.-H., Jung, Y.-R., & Kim, S.-B. (2015). Experimental study on artificial supercavitation of the high speed torpedo. *Journal of the Korea Institute of Military Science and Technology, 18*(3), 300-308.

Alyanak, E., Grandhi, R., & Penmetsa, R. (2006). Optimum design of a supercavitating torpedo considering overall size, shape, and structural configuration. *International Journal of Solids and Structures, 43*(3-4), 642-657.

Amromin, E. (2007). Analysis of body supercavitation in shallow water. *Ocean Engineering, 34*(11-12), 1602-1606.

Chung, J., & Cho, Y. (2015). Visualization of ventilated supercavitation phenomena around a moving underwater body. *Journal of the Korean Society of Visualization, 13*(1), 26-29.

Gong, B.-Z., Zhang, B.-J., & Zhang, H. (2008). NEMD study for supercavitation mechanism with underwater object. *Physics Letters A, 372*(47), 7063-7067.

Javadpour, S. M., Farahat, S., Hossein, A., Salari, M., & Nezhad, A. H. (2017). Experimental and numerical study of ventilated supercavitation around a cone cavitator. *Heat and Mass Transfer, 53*(5), 1491-1502.

Jia, L.-p., Wang, C., Wei, Y.-j., Wang, H.-b., Zhang, J.-z., & Yu, K.-p. (2006). Numerical simulation of artificial ventilated cavity*. *Journal of Hydrodynamics, Ser. B, 18*(3), 273-279.

Jiang, C.-X., Shuai, Z.-J., Zhang, X.-Y., Li, W.-Y., & Li, F.-C. (2016). Numerical study on evolution of axisymmetric natural supercavitation influenced by turbulent drag-reducing additives. *Applied Thermal Engineering, 107*, 797-803.

Jiang, Y., Bai, T., & Gao, Y. (2017). Formation and steady flow characteristics of ventilated supercavity with gas jet cavitator. *Ocean Engineering, 142*, 87-93.

Karn, A., & Rosiejka, B. (2017). Air entrainment characteristics of artificial supercavities for free and constrained closure models. *Experimental Thermal and Fluid Science, 81*, 364-369.

Karn, A., Arndt, R. E., & Hong, J. (2015). Dependence of supercavity closure upon flow unsteadiness. *Experimental Thermal and Fluid Science, 68*, 493-489.

Khoo, B., & Zheng, J. (2013). Force analysis of underwater object with supercavitation evolution. *Indian Journal of Geo-Marine Sciences, 42*(8), 957-963.

Kim, B.-J., Choi, J.-K., & Kim, H.-T. (2015). An experimental study on ventilated supercavitation of the disk cavitator. *Journal of the Society of Naval Architects of Korea, 52*(3), 236-247.

Kinzel, P., M., Krane, M. H., Kirschner, I. N., & Moeny, M. J. (2017). A numerical assessment of the interaction of a supercavitating flow with a gas jet. *Ocean Engineering, 136*, 304-313.

May, A. (1975). *WATER ENTRY AND THE CAVITY-RUNNING BEHAVIOR OF MISSILES.* Defense Technical Information Center.

Moghimi, M., Nouri, N. M., & Molavi, E. (2017). Experimental Investigation on Supercavitating Flow over Parabolic Cavitators. *Journal of Applied Fluid Mechanics, 10*(1), 95-102.

Nouri, N. M., Riahi, M., Valipour, A., Raeyatpishe, M. M., & Molavi, E. (2015). Analytical and experimental study of hydrodynamic and hydroacoustic effects of air injection flow rate in ventilated supercavitation. *Ocean Engineering, 95*, 94-105.

Pendar, M., & Roohi, E. (2015). Detailed investigation of cavitation and supercavitation around different geometries using various turbulence and mass transfer models. *Journal of Physics: Conference Series*, *656.*

Roohi, E., Zahiri, A. P., & Passandideh-Fard, M. (2013). Numerical simulation of cavitation around a two-dimensional hydrofoil using VOF method and LES turbulence model. *Applied Mathematical Modeling, 37*(9), 6469-6488.

Saranjam, B. (2013). Experimental and numerical investigation of an unsteady supercavitating moving body. *Ocean Engineering, 59*, 9-14.

Schlichting, H., & Gersten, K. (2001). Boundary-Layer Theory. *European Journal of Mechanics - B/Fluids*. doi:10.1016/S0997-7546(00)01101-8

Serebryakov, V., Arndt, R., & Dzielski, J. (2015). Supercavitation: Theory, experiment and scale effects. *Journal of Physics: Conference Series*, *656.*

Shahr-e-Babaki, M. G., Keikha, A. J., & Mehr, A. B. (2017). Effect of injection angle on artificial cavitation using the design of experiment method. *Journal of Marine Science and Application, 16*(2), 173-181.

Shang, Z. (2013). Numerical investigations of supercavitation around blunt bodies of submarine shape. *Applied Mathematical Modeling, 37*(20-21), 8836-8845.

Shao, S., Karn, A., Ahn, B.-K., Arndt, R. E., & Hong, J. (2017). A comparative study of natural and ventilated supercavitation across two closed-wall water tunnel facilities. *Experimental Thermal and Fluid Science, 88*, 519-529.

Skidmore, G. M., Brungart, T. A., Lindau, J. W., & Moeny, M. J. (2016). The control of ventilated supercavity pulsation and noise. *International Journal of Multiphase Flow, 85*, 14-22.

Vanek, B., Bokor, J., Balas, G. J., & Arndt, R. E. (2007). Longitudinal motion control of a high-speed supercavitation vehicle. *Journal of Vibration and Control, 13*(2), 159+.

Weiland, C., & Vlachos, P. P. (2012). Time-scale for critical growth of partial and supercavitation development over impulsively translating projectiles. *International Journal of Multiphase Flow, 38*(1), 73-86.

Yang, D., Xiong, Y., & Guo, X. (2017). Drag reduction of a rapid vehicle in supercavitating flow. *International Journal of Naval Architecture and Ocean Engineering, 9*(1), 35-44.

Yang, W., Yang, Z., Wen, K., Yang, Z., & Zhang, Y. (2016). Numerical investigation on the gas entrainment rate on ventilated supercavity body. *The Journal of Computational Multiphase Flows, 8*(4), 169-177.

Yudaev, V. (2015). The limits of operation modes for apparatuses with cavitation excitation. *Theoretical Foundations of Chemical Engineering, 49*(1), 90-94.

Zhang, X.-w., Wei, Y.-j., Zhang, J.-z., Wang, C., & Yu, K.-p. (2007). Experimental research on the shape characters of natural and ventilated supercavitation. *Journal of Hydrodynamics, Ser. B, 19*(5), 564-571.

Appendix A – Mesh Independence Study Permutations

#	Inlet velocity	Time step	Torpedo body sizing element size	Mesh max face size	Mesh size ratio
Units	m/s	s	mm	m	
DP 0	75	6.67E-06	1	0.005	5
DP 1	75	6.67E-06	1	0.00707	7.07
DP 2	75	6.67E-06	1	0.01	10
DP 3	75	6.67E-06	1	0.01414	14.14
DP 4	75	6.67E-06	1	0.02	20
DP 5	75	6.67E-06	1	0.02828	28.28
DP 6	75	6.67E-06	1	0.04	40
DP 7	75	4.71E-06	0.707	0.003535	5
DP 8	75	4.71E-06	0.707	0.00499849	7.07
DP 9	75	4.71E-06	0.707	0.00707	10
DP 10	75	4.71E-06	0.707	0.00999698	14.14
DP 11	75	4.71E-06	0.707	0.01414	20
DP 12	75	4.71E-06	0.707	0.01999396	28.28
DP 13	75	4.71E-06	0.707	0.02828	40
DP 14	75	3.33E-06	0.5	0.0025	5
DP 15	75	3.33E-06	0.5	0.003535	7.07
DP 16	75	3.33E-06	0.5	0.005	10
DP 17	75	3.33E-06	0.5	0.00707	14.14
DP 18	75	3.33E-06	0.5	0.01	20
DP 19	75	3.33E-06	0.5	0.01414	28.28
DP 20	75	3.33E-06	0.5	0.02	40
DP 21	75	2.36E-06	0.354	0.00531	15
DP 22	75	1.67E-06	0.25	0.00375	15